



Numerical solution of Boussinesq systems of KdV–KdV type: II. Evolution of radiating solitary waves

To cite this article: J L Bona *et al* 2008 *Nonlinearity* **21** 2825

View the [article online](#) for updates and enhancements.

Related content

- [Boussinesq equations and other systems](#)
J L Bona, M Chen and J-C Saut
- [Evolution and stability \$\Phi^4\$ oscillators](#)
L Arturo Ureña-López, Susana Valdez-Alvarado and Ricardo Becerril
- [PROPAGATION AND DISPERSION OF TRANSVERSE WAVE TRAINS IN MAGNETIC FLUX TUBES](#)
R. Oliver, M. S. Ruderman and J. Terradas

Recent citations

- [Scattering of bulk strain solitary waves in bi-layers with delamination](#)
K.R. Khusnutdinova and M.R. Tranter
- [An ADER-type scheme for a class of equations arising from the water-wave theory](#)
G.I. Montecinos *et al*
- [Petviashvili type methods for traveling wave computations: II. Acceleration with vector extrapolation methods](#)
J. Álvarez and A. Durán

Numerical solution of Boussinesq systems of KdV–KdV type: II. Evolution of radiating solitary waves

J L Bona¹, V A Dougalis^{2,3} and D E Mitsotakis^{2,3}

¹ Department of Mathematics, Statistics and Computer Science, University of Illinois at Chicago, Chicago IL 60607, USA

² Department of Mathematics, University of Athens, 15784 Zographou, Greece

³ Institute of Applied and Computational Mathematics, FO.R.T.H., PO Box 1527, 71110 Heraklion, Greece

E-mail: bona@math.uic.edu, doug@math.uoa.gr and dmitsot@math.uoa.gr

Received 10 January 2008, in final form 10 August 2008

Published 13 November 2008

Online at stacks.iop.org/Non/21/2825

Recommended by A L Bertozzi

Abstract

In this paper we consider a coupled KdV system of Boussinesq type and its symmetric version. These systems were previously shown to possess generalized solitary waves consisting of a solitary pulse that decays symmetrically to oscillations of small, constant amplitude. We solve numerically the periodic initial-value problem for these systems using a high order accurate, fully discrete, Galerkin-finite element method. (In the case of the symmetric system, it is possible to prove rigorous, optimal-order, error estimates for this scheme.) The numerical scheme is used in an exploratory fashion to study radiating solitary-wave solutions of these systems that consist, in their simplest form, of a main, solitary-wave-like pulse that decays asymmetrically to small-amplitude, outward-propagating, oscillatory wave trains (ripples). In particular, we study the generation of radiating solitary waves, the onset of ripple formation and various aspects of the interaction and long time behaviour of these solutions.

Mathematics Subject Classification: 35Q53, 65M60, 65M15, 76B15, 76B25

1. Introduction

In a previous paper [13], the present authors considered systems of the Boussinesq type, including the *KdV–KdV system* [9, 10]

$$\begin{aligned} \eta_t + u_x + (\eta u)_x + \frac{1}{6}u_{xxx} &= 0, \\ u_t + \eta_x + uu_x + \frac{1}{6}\eta_{xxx} &= 0, \end{aligned} \tag{1.1}$$

and the *symmetric KdV–KdV system*, [11],

$$\begin{aligned}\eta_t + u_x + \frac{1}{2}(\eta u)_x + \frac{1}{6}u_{xxx} &= 0, \\ u_t + \eta_x + \frac{1}{2}\eta\eta_x + \frac{3}{2}uu_x + \frac{1}{6}\eta_{xxx} &= 0.\end{aligned}\tag{1.2}$$

The variables in these systems are non-dimensional, but unscaled. Both systems are approximations to the two-dimensional Euler equations for surface wave propagation along a horizontal channel that contains an ideal fluid. Both admit two-way wave propagation and are valid approximations to the Euler equations in the case of long waves of small amplitude, when the Stokes number of the flow is of $O(1)$ [9, 11]. The independent variable x represents the position along the channel, t is proportional to time, $\eta(x, t)$ is the deviation of the free surface from its undisturbed level at (x, t) , while $u(x, t)$ is the horizontal velocity at (x, y, t) , where y is the dimensionless height $\sqrt{2/3}$ above the bottom. (The undisturbed depth is equal to one in the present variables.) The system (1.1) is one of the systems put forth in [9]. It has a Hamiltonian structure and its initial-value problem has been shown in [10] to be well posed, locally in time, in appropriate Sobolev classes. The symmetric system (1.2) is one of the family of systems derived in [11] and reduces to a symmetric hyperbolic system when the dispersive terms are dropped. A local well-posedness theory for the initial-value problem for (1.2) in appropriate Sobolev spaces was also developed in [11]. Its solution conserves the L^2 -norm, which is to say, the quantity $\int_{-\infty}^{\infty} (\eta^2 + u^2) dx$ does not depend upon t .

Since the systems (1.1) and (1.2) are approximations to the Euler equations, a natural question to ask is whether they possess solitary-wave solutions like those of the Euler equations. In [13], using the theory of [26], we showed that (1.1) and (1.2) do not possess classical solitary waves decaying to zero at infinity (with the possible exception of isolated, ‘embedded’ solitary waves). Instead, they possess generalized solitary waves (GSW), which are homoclinic to periodic solutions of small amplitude. Such GSW have been shown to exist as travelling-wave solutions of gravity-capillary surface wave models and various other model equations and systems arising in water-wave theory (see, e.g. [3, 5, 6, 16, 17, 19, 22, 25–27, 30, 31] and their references). In [13] we constructed accurate approximations to GSW solutions of (1.1) and (1.2) by solving numerically periodic boundary-value problems for the nonlinear systems of ordinary differential equations satisfied by travelling-wave solutions of the systems. We then checked, using these GSWs as initial conditions in an evolution code approximating the periodic initial-value problem for the systems, that they indeed travelled with practically constant speed and shape over very long temporal intervals.

The GSWs are solutions of (1.1) or (1.2) on the real line, whose L^2 -norm is infinite. When initial conditions of finite energy, i.e. functions $\eta(x, 0)$ and $u(x, 0)$ vanishing sufficiently fast at infinity, are allowed to evolve under (1.1) or (1.2), what is observed numerically is that the solution forms wavetrains that travel in both directions. These wavetrains typically consist of one or more main pulses that resemble classical solitary waves and are followed by dispersive oscillatory tails of small amplitude. What is also observed is that oscillations of very small amplitude (ripples) are immediately formed and propagate outwards, preceding and travelling faster than the largest of the main pulses. (This effect of radiation of ripples by solitary waves was first observed in [6], to our knowledge, in the context of a one-way model.) The solitary-wave-like pulses apparently decay in amplitude and speed; it appears that their energy is being transferred to the ripples. They will be called in the following ‘radiating solitary waves’ although they are not proper solitary waves as they do not travel with constant speed and shape.

The existence of GSWs and of radiating solitary waves has been observed and studied in the case of the *fifth-order KdV equation*

$$u_t + uu_x + u_{xxx} + u_{xxxxx} = 0,$$

see, e.g. [4, 6, 15–17, 23, 29, 32]. The above equation is a unidirectional model for small-amplitude gravity-capillary wave propagation in a certain range of Bond numbers, see [24]. It possesses GSW solutions (see, e.g. [4] for a summary and references to the relevant existence theory established by dynamical systems techniques), whose decay to exponentially small oscillatory profiles extending symmetrically to infinity from both ends of the main pulse was studied by asymptotic techniques (when the fifth-order derivative is multiplied by a small positive parameter) in [15, 23, 29, 32], among others, and numerically in many other works starting with [15]. It was recognized in [6] that this equation possesses asymmetric solutions that are not travelling waves, and in which a main, solitary-wave-like pulse decays asymmetrically to rightward propagating ripples that are generated at the front of this pulse. These solutions were studied by numerical and asymptotic methods in [6, 4].

In this paper, we study by numerical means certain properties of solutions of (1.1) and (1.2), especially issues connected with the generation and evolution of radiating solitary waves. Light shed on these issues gives information about the long-term programme of understanding how nonlinearity and dispersion interact with one another, in addition to providing a more detailed view of the particular systems (1.1) and (1.2). We consider the periodic initial-value problem for (1.1) and (1.2) on a spatial interval $[a, b]$, on which we suppose that the initial conditions

$$\eta(x, 0) = \eta_0(x), \quad u(x, 0) = u_0(x), \quad x \in [a, b], \quad (1.3)$$

hold. Here η_0, u_0 are smooth, periodic, real-valued functions on $[a, b]$. We assume that the periodic initial-value problems (1.1)–(1.3) and (1.2)–(1.3) have unique smooth solutions over a temporal interval $[0, T]$. While interest is focused mainly on what happens to localized disturbances η_0 and u_0 when (1.1) or (1.2) is considered posed on the whole real line \mathbb{R} , it is the periodic initial-value problem that is actually approximated numerically. The presumption, which has been backed up by rigorous theory in related situations (see, e.g. [7, 18]), is that if the interval $[a, b]$ is large compared with the support of η_0 and u_0 , then, at least over a certain time interval, the solution of the problem considered on \mathbb{R} and the solution of the periodic initial-value problem closely agree, at least on the fundamental period domain.

The plan of the paper is as follows. In section 2 the fully discrete numerical schemes used in the simulations are outlined. For the spatial discretization of (1.1) and (1.2) a standard Galerkin-finite element method is used, with smooth periodic splines on a uniform mesh. The resulting semi-discrete systems of ordinary differential equations are very stiff and are discretized in time by the fourth-order accurate, two-stage implicit Runge–Kutta method of the Gauss–Legendre type. This type of scheme has been previously used for simulating accurately various nonlinear dispersive KdV-type equations (see, e.g. [12, 21]) without requiring stringent stability conditions on the discretization parameters. For the KdV–KdV systems (1.1) and (1.2), the implementation of this implicit scheme requires solving at each time step nonlinear systems of equations. Solutions of these are approximated by Newton’s method. The attendant linear systems are solved efficiently by iterative methods in the spirit of the analogous technique for the KdV equation in [12]; here, its application to systems requires new twists. The resulting fully discrete scheme was tested and found experimentally to be of optimal order of accuracy in [13]. An optimal-order L^2 error estimate for the semi-discrete approximation of the periodic initial-value problem for the symmetric KdV–KdV system (1.2) has been proved in [21]. An analogous result for the semi-discretization of (1.1), which is much harder to analyse, is not yet available, though our simulations show that the scheme has optimal-order L^2 -convergence rates.

In section 3, this numerical scheme is used to simulate the evolution, under (1.1), of a ‘heap of water’ modelled by a Gaussian initial surface elevation and zero initial velocity.

This corresponds to earlier numerical experiments (see [28], for example). The initial profile resolves into right- and left-going waves composed of radiating solitary pulses followed by a dispersive tail and preceded by ripples. The ripples eventually wrap around the boundary due to periodicity and superimpose themselves on the rest of the wave profile. Following the ideas in [8], a procedure is initiated for ‘cleaning’ the main pulses. This procedure does not clear out the ripples, which are a permanent feature of the solution of the KdV–KdV systems. We study their development and growth.

A further numerical study of the generation and evolution of radiating solitary waves is performed in section 4 on larger spatial intervals and with special initial data that yield nearly one-way propagating waves as in [1]. In these experiments, the aim is to simulate more accurately the initial stages of the evolution of the Cauchy problem for the KdV–KdV systems. In particular, we describe in detail the onset of the ripples and the decay in amplitude and energy of the main pulses, paying particular attention to recording the amplitude of the generated ripples as a function of the amplitude of the initial main pulse. Finally, Section 5 addresses several issues of longer-time evolution, ‘stability’ and interaction of radiating solitary waves. Among other points of interest, there emerges the interesting fact that GSWs, when perturbed or when they collide, apparently lose their travelling-wave character and start radiating.

What is found is rather interesting. First, while there are no solitary-wave solutions of finite energy of these KdV–KdV systems, there are nevertheless ‘ghosts’ of such solutions that play the same role as do the classical solitary-wave solutions of other Boussinesq systems (see [20, 28]). That is, initial disturbances of finite energy try to break up into solitary waves, but succeed only in forming a train of these radiating solitary waves. The radiating solitary waves are not stable, but they appear to hold their identity well enough through interactions and under perturbations to be loosely termed meta-stable. On very long time scales, the conjecture that is forced upon us is that all initial data will disperse due to the lack of coherent structures of finite energy to which the solutions can evolve. These time scales are much longer than the time scale over which the systems (1.1) and (1.2) are proven to be good approximations of the two-dimensional Euler system, but if this proposition were established, it would argue against the use of (1.1) and (1.2) in practical water-wave simulations.

By and large, the systems (1.1) and (1.2) give qualitatively similar results for the range of phenomena described in this paper. There are a few interesting differences however, which are pointed out along the way. It is worth noting that the numerical scheme used is more robust in the case of the symmetric system (1.2).

2. The numerical scheme

This section provides a brief review of the fully discrete Galerkin-finite element scheme that is used to discretize the periodic initial-value problem for the systems (1.1) and (1.2).

To describe the discretization in the spatial variable x , let N be a positive integer and define a uniform grid on $[a, b]$ by $x_j := jh$, $0 \leq j \leq N$, where $h := (b - a)/N$. For integers $r \geq 3$, consider the N -dimensional space S_h^r of smooth periodic splines of order r (degree $r - 1$) defined as

$$S_h^r := \{\phi \in C_p^{r-2}([a, b]) : \phi|_{[x_j, x_{j+1}]} \in \mathbb{P}_{r-1}, j = 0, 1, \dots, N - 1\},$$

where $C_p^k([a, b])$ denotes the k times continuously differentiable, periodic functions on $[a, b]$. The *standard Galerkin semi-discrete approximations* of the solutions of the periodic

initial-value problems (1.1)–(1.3) and (1.2)–(1.3) are the pairs of S_h^r -valued functions η_h, u_h defined on some temporal interval $[0, t^*]$ by the following equations.

- For the KdV–KdV system (1.1):

$$\begin{aligned} \langle \eta_{ht}, \chi \rangle + \langle u_{hx} + (\eta_h u_h)_x, \chi \rangle - \frac{1}{6} \langle u_{hxx}, \chi_x \rangle &= 0, \\ \langle u_{ht}, \psi \rangle + \langle \eta_{hx} + u_h u_{hx}, \psi \rangle - \frac{1}{6} \langle \eta_{hxx}, \psi_x \rangle &= 0, \end{aligned} \quad \forall \chi, \psi \in S_h^r, \quad 0 \leq t \leq t^*, \tag{2.1}$$

- For the symmetric KdV–KdV system (1.2):

$$\begin{aligned} \langle \eta_{ht}, \chi \rangle + \langle u_{hx} + \frac{1}{2}(\eta_h u_h)_x, \chi \rangle - \frac{1}{6} \langle u_{hxx}, \chi_x \rangle &= 0, \\ \langle u_{ht}, \psi \rangle + \langle \eta_{hx} + \frac{1}{2}\eta_h \eta_{hx} + \frac{3}{2}u_h u_{hx}, \psi \rangle - \frac{1}{6} \langle \eta_{hxx}, \psi_x \rangle &= 0, \end{aligned} \quad \forall \chi, \psi \in S_h^r, \quad 0 \leq t \leq t^*. \tag{2.2}$$

Here, $\langle \cdot, \cdot \rangle$ denotes the inner product on the space $L^2(a, b)$. (The corresponding L^2 -norm will be denoted by $\| \cdot \|$.) The systems (2.1) and (2.2) are supplemented by the initial values

$$\eta_h(0) = P_h \eta_0, \quad u_h(0) = P_h u_0, \tag{2.3}$$

where P_h is the L^2 -projection operator on S_h^r . It is readily seen that (2.1) and (2.2) comprise first-order, $N \times N$ nonlinear systems of ordinary differential equations. The initial-value problems (2.1)–(2.3) and (2.2)–(2.3) have solutions that exist at least locally in time, on intervals $[0, t^*]$, where $t^* = t^*(h)$.

The symmetric KdV–KdV system (1.2) has a number of favourable mathematical properties, when compared with the system (1.1). Some of these properties, for example, the conservation of the L^2 -norm of the solution (η, u) of (1.2)–(1.3) on its temporal interval of existence $[0, T]$,

$$\frac{d}{dt} (\|\eta\|^2 + \|u\|^2) = 0, \quad 0 \leq t \leq T,$$

also hold for the solution (η_h, u_h) of the corresponding semi-discretization (2.2)–(2.3). In [21] it is proved that the temporal interval of existence of (η_h, u_h) is at least equal to $[0, T]$ and that the optimal-order L^2 error estimate

$$\max_{0 \leq t \leq T} (\|\eta - \eta_h\| + \|u - u_h\|) \leq ch^r \tag{2.4}$$

holds for some constant $c = c(\eta, u, T)$, independent of h , if the solution (η, u) of (1.2)–(1.3) is sufficiently smooth. We have not been able to prove analogous error estimates for the system (1.1). However, in [13], we have verified by means of numerical experiments the validity of (2.4) for the system (1.1) in the cases of cubic and quintic splines, i.e. for $r = 4$ and 6.

The systems of ordinary differential equations (2.1) and (2.2) are very stiff. To discretize them stably in the temporal variable, an implicit time stepping scheme is mandated. We resorted in [13] to the fourth-order accurate, two-stage Gauss–Legendre implicit Runge–Kutta method, which, as is well known, has favourable nonlinear stability properties. This scheme, being fully implicit, requires that a $2N \times 2N$ nonlinear system of equations be solved at each time step. We accomplish this using Newton’s method in the spirit of [12]; the attendant linear systems of equations are solved iteratively by an ‘inner’ iteration procedure that requires at a given time step, solving a number of $N \times N$ complex, sparse linear systems with the same matrix. The overall fully discrete method appears to be unconditionally stable and has global L^2 error bounds of order $O(k^4 + h^r)$, where k is the uniform time step. This was checked by means of numerical experiments for both KdV–KdV systems in [13].

3. Application of a ‘cleaning’ procedure to KdV–KdV systems

If the periodic initial-value problem for (1.1) or (1.2) is initiated with given localized initial profiles (η_0, u_0) resembling a ‘heap’ of water and its solution approximated using the evolution code described in section 2, one observes that one or more solitary-wave-like pulses are generated, followed by smaller amplitude dispersive oscillatory tails and accompanied by very small-amplitude oscillations (ripples). This is illustrated, for example, in figures 4(a) and (b), which show the right-travelling wavetrain (there is also a companion, left-travelling wavetrain which has been cut out) produced at $t = 160$ by the evolution according to (1.1), generated by a Gaussian initial surface elevation profile and zero initial velocity. More precisely, the initial data that generated the outcome of figure 4 were

$$\eta_0(x) = 0.3e^{-(x+100)^2/25}, \quad u_0(x) = 0, \quad x \in [-150, 150]. \quad (3.1)$$

To study the question of possible generation of travelling waves from the initial profile (2.1) under the evolutions (1.1) and (1.2), use is made of the ‘cleaning’ process put forward in [8] in a similar context. The idea is to let the leading solitary elevation distance itself from the trailing dispersive tails, which it will on account of their differing dynamics, and then cut this pulse from the rest and use it anew as an initial value. The new structure, while not yet an exact travelling wave, will develop a smaller dispersive tail which can again, after due lapse of time in the evolution, be clipped from a newly arisen solitary pulse. Repeating this process several times was observed in [8] to result in a very good approximation of a travelling-wave solution of the relevant evolution equations. For Boussinesq systems that feature bounded group and phase velocities, such as those studied in [2, 8, 20], this procedure seems to work rather well, generating in a few iterations travelling-wave profiles with noise amplitude of only about 10^{-10} . For (1.1) and (1.2), the procedure is complicated by the fact that the expected solitary-wave-like pulses are accompanied by ripples and the fact that the group and phase velocities are unbounded. (If $\omega(\kappa)$ is the frequency associated via the linearized dispersion relation with wavenumber κ , then the group velocity $\omega'(\kappa)$ grows like $\pm\kappa^2/2$ as wavenumbers get large.)

To get an idea of how well the cleaning process works in the context of unbounded group and phase velocities, it is informative to apply it first to the Korteweg–de Vries equation

$$u_t + u_x + uu_x + \frac{1}{6}u_{xxx} = 0, \quad (3.2)$$

where one understands in detail the travelling waves and where there are no GSWs.

The solution of (3.2) on the interval $[-150, 150]$ with periodic boundary conditions was approximated using cubic splines with $h = 0.1$ and the two-stage Gauss–Legendre Runge–Kutta time-stepping scheme with $k = 0.02$, starting from the Gaussian $u(x, 0) = 0.5e^{-(x+100)^2/25}$. In the first cleaning iteration, we let the solution evolve up to $t = 160$ (cf figure 1), cut the dispersive tail by setting $u_h = 0$ in the two intervals $[-150, 90.2]$, $[113.2, 150]$ and translated back the remaining pulse so that its peak was again at $x = -100$. (It should be noted that ‘cutting’, i.e. setting the numerical solution equal to zero in a set $[-150, \alpha] \cup [\beta, 150]$, is done smoothly by setting the coefficients of the B-spline basis functions in the representation of u_h equal to zero before and after some index, see figure 1(c).) Thus the truncated solution is in $C^2([-150, 150])$. During the evolution from the new initial profile, small-amplitude oscillations were still produced behind the main wave due to the cutting, so the process had to be repeated. The amplitude of the oscillatory noise decreased rather slowly as a function of the number of cleaning iterations. For example, figure 2 shows three stages of cleaning the solitary wave. However, the cleaning procedure is apparently convergent: the ‘clean’ solitary wave that is produced after 15 cleaning iterations propagates over a long time interval (up to

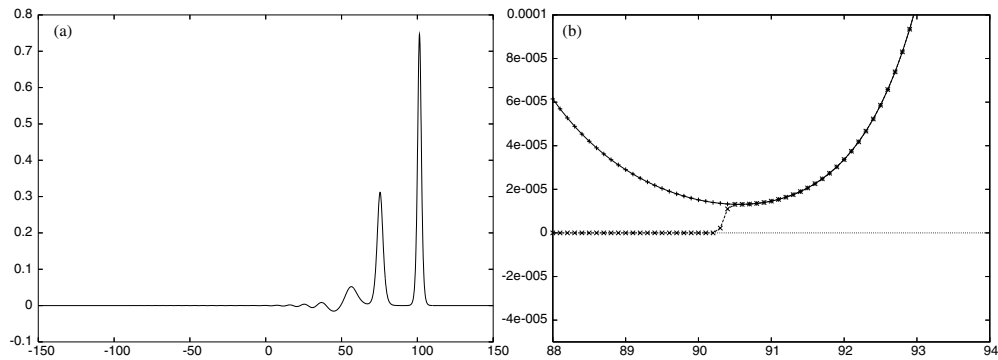


Figure 1. (a) Evolution of a Gaussian, KdV equation (3.2), $t = 160$; (b) smooth truncation in the vicinity of $x = -90.2$.

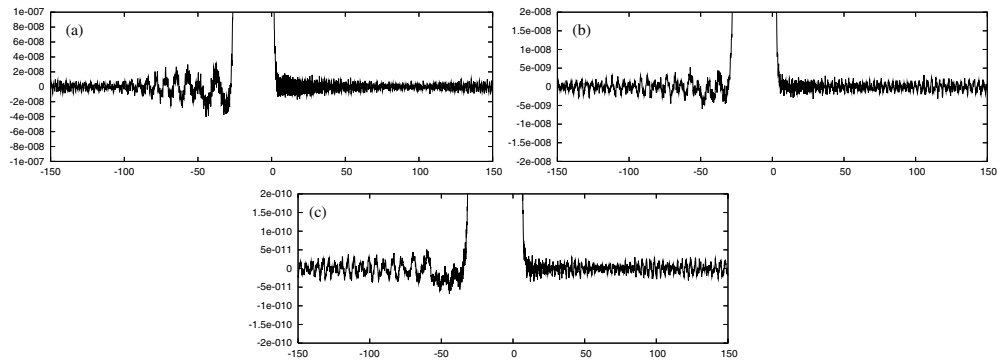


Figure 2. Cleaning of the cut solitary wave of figure 1. (a) After the 4th iteration, (b) after the 7th iteration, (c) after the 15th iteration. (All at $t = 70$.)

$t = 200$ at least) with a speed (1.249 12) and an amplitude (0.747 367) that are constant to six digits, and an L^2 -shape error (relative to its shape at $t = 0$) less than 3.7×10^{-6} .

Having convinced ourselves that the cleaning procedure works even in the face of unbounded group velocities, we proceeded to integrate the KdV–KdV system (1.1) with the evolution code described in section 2, using cubic splines with $h = 0.02$, $k = 0.004$ on $[-150, 150]$ and with initial conditions given by (3.1). The aim was to produce a ‘clean’ travelling wave-like solution. The initial profile resolves into two wavetrains moving in opposite directions; figures 3(a) and (b) show the η component of this solution at $t = 30$. Note that in addition to the dispersive tails following the two main pulses, small-amplitude ripples have developed in front of the main pulses. The wave is then cleaned, keeping only the rightward moving wavetrain, by setting the solution equal to zero in $[-150, -100.6] \cup [50.44, 150]$ and using the resulting η_h and u_h as new initial conditions for the system, setting $t = 0$ again. At $t = 160$ this solution has evolved into one whose η -component is shown in figures 4(a) and (b). (Note the ripples that have appeared again.) This solution is translated so its maximum is at $x = -50$ and is cleaned in $[-150, -117.26] \cup [-36.3, 150]$. The result for the η -component is shown in figure 4(c). This procedure is repeated two more times. After the fourth cleaning, the solution is evolved up to $t = 70$; the η -component is shown in figures 5(a) and (b). At this point, the leading pulse has distanced itself sufficiently from the trailing dispersive tail. Hence, after translating back so that the maximum is at $x = -100$,

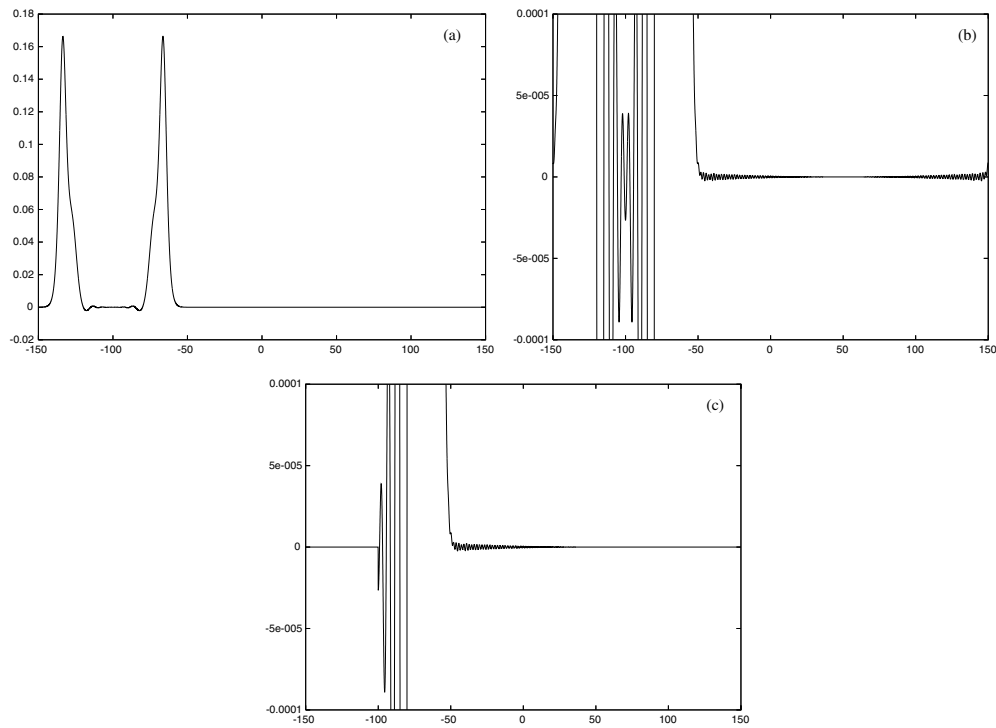


Figure 3. Evolution of a Gaussian, system (1.1), η at $t = 30$; (b) is a magnification of (a) and (c) is the new initial profile after the first cleaning.

the main pulse is again isolated by cutting out dispersive tails and ripples i.e. zeroing the solution in $[-150, -114.4] \cup [-86.44, 150]$ (fifth cleaning). The resulting η -pulse is shown in figure 5(c).

If this profile is now evolved, the resulting dispersive tail is negligible; however, ripples appear again in front of the main pulse and wrap around due to periodicity. If the solution is cleaned two more times and the evolution code started from the profile whose η -component is shown in figure 6(a), there obtains the evolution shown in figures 6(b)–(j) up to $t = 700$. Ripples develop in front of the wave, wrap around the boundary due to periodicity and ‘climb over’ the main pulse. Up to $t = 700$ they seem to stabilize around an amplitude of 5×10^{-5} .

These ripples do not appear to be an artefact of the numerical integration. When the computation is repeated with smaller h and k , and also when quintic splines are used for the spatial discretization and a different time-stepping method implemented (a third-order accurate Gauss–Lobatto implicit Runge–Kutta scheme), there obtains, at the same cleaning level, exactly the same profile. The profile of the ripples changes with the number of cleanings of course, but it is convergent and by the seventh cleaning it has stabilized. Figure 7, for example, gives some idea of this convergence; it shows the ripples after the sixth cleaning (dotted line) and after the seventh cleaning (solid line) at $t = 120$. The profile after the eighth cleaning is identical within line thickness to that after the seventh cleaning. Thus, it is reasonable to conclude that after the seventh cleaning, the noise due to the cleaning process has fallen to at least two orders of magnitude below the level of the ripples.

The ripples at $t = 120$, see figure 7, have a maximum amplitude (after the seventh cleaning) of about 4×10^{-5} . We measured their propagation speed and period at different subintervals of

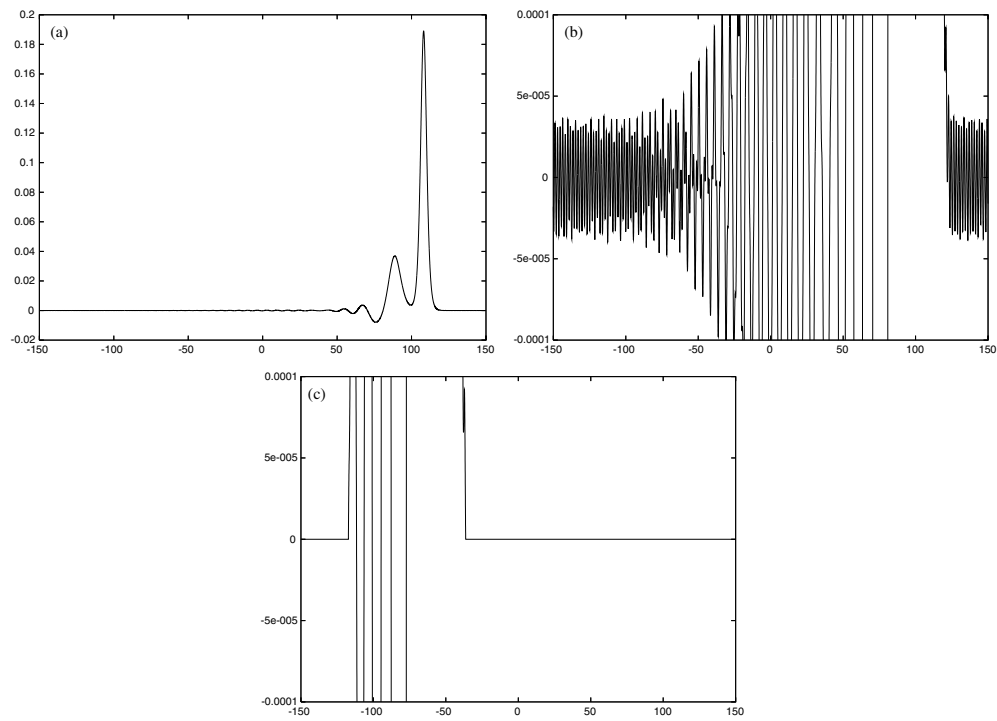


Figure 4. Evolution of η -profile (c) of figure 3, $t = 160$; (b) is a magnification of (a) and (c) is the new initial profile after translation and the second cleaning.

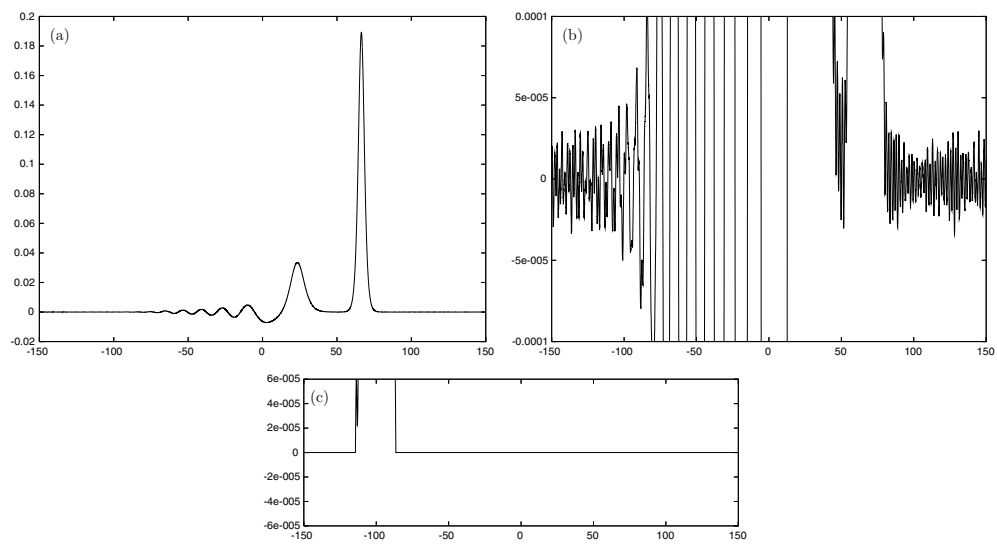


Figure 5. Evolution after the fourth cleaning, $t = 70$; (b) is a magnification of (a) and (c) is the new initial profile after translation and the fifth cleaning.

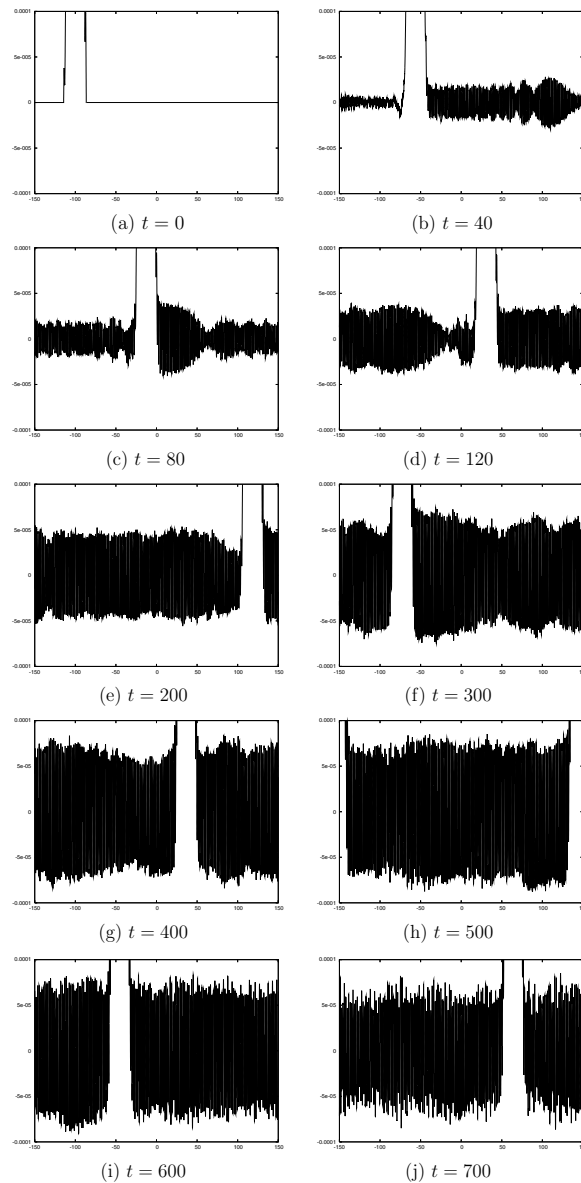


Figure 6. Evolution of the η -component after the seventh cleaning. (a) $t = 0$, (b) $t = 40$, (c) $t = 80$, (d) $t = 120$, (e) $t = 200$, (f) $t = 300$, (g) $t = 400$, (h) $t = 500$, (i) $t = 600$ and (j) $t = 700$.

$[-150, 150]$ and found that the ripples are very nearly solutions of the linearized system. For example, in the case of the ripples of figure 7(e), the measured average spatial period was equal to about 1.77 (hence $\kappa \cong 3.55$) and the average phase speed was about 1.11. (The wave number computed for this speed from the linearized dispersion relation for (1.1), $\kappa = \sqrt{6(c+1)}$, is equal to about 3.56.)

The properties of the main pulse are not easy to measure due to the superposition of ripples on it. The variation of the amplitude of its η -component and of the speed of the pulse with

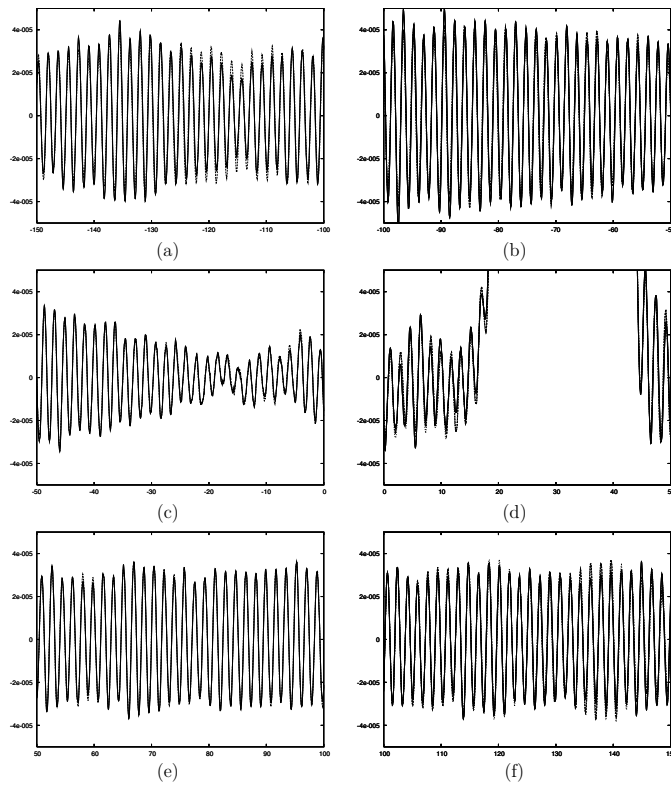


Figure 7. Magnification of the ripples; $t = 120$, (—) 7th cleaning, (---) 6th cleaning.

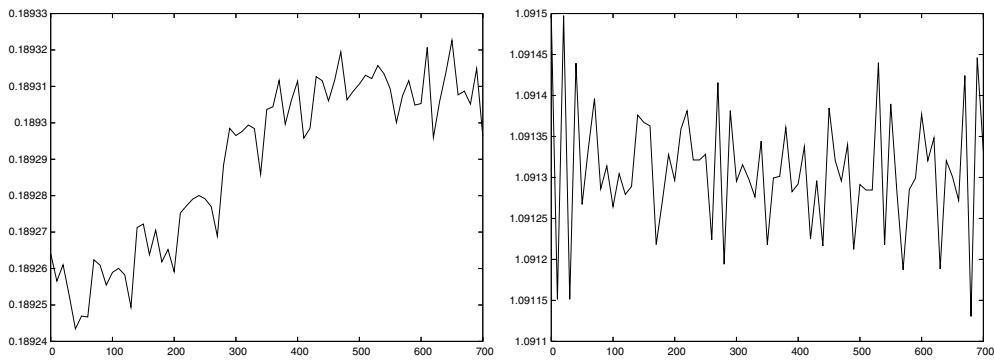


Figure 8. Amplitude (left) and speed (right) of the main pulse of figure 6 as functions of t .

time is shown in figure 8. The amplitude seems to stabilize around the value 0.18931 ± 10^{-5} , while the speed is about $1.0913 \pm 2 \times 10^{-4}$.

Overall, the computation was of quite good quality. The invariants $I_1 = \int u \, dx$, $I_2 = \int \eta \, dx$, $I_3 = \int \eta u \, dx$ of (1.1) were conserved up to 10, 9 and 9 digits, respectively, up to $t = 700$. The Hamiltonian $H = \int [\frac{1}{6}\eta_x^2 + \frac{1}{6}u_x^2 - \eta^2 - u^2(1 + \eta)] \, dx$ was preserved to 5 digits up to $t = 170$ and to 4 digits up to $t = 700$.

A qualitatively similar picture was observed when the ‘cleaning’ procedure was applied to the evolution generated from the initial conditions (3.1) by the periodic initial-value problem for the symmetric KdV–KdV system (1.2). The main difference was the larger size of the amplitude of the ripples.

It is tentatively concluded that in the case of the KdV–KdV systems, the cleaning procedure does not yield ‘clean’ solitary-wave pulses as in the KdV equation or alternative Boussinesq systems. This is of course due to the fact that the KdV–KdV systems do not possess classical solitary-wave solutions as was pointed out in [13]. In the case of system (1.1), as shown in figures 6(a) and (b), when an isolated rightward-travelling η -pulse (obtained in our case by a previous iteration of cleaning and smooth truncation) is used as an initial condition for (1.1) with its associated velocity u , it moves to the right radiating rightward-travelling, small-amplitude ripples from its front. (The leftward-travelling part of the solution radiates leftward-travelling ripples from its front. Hence the ripples travel outwards from the bulk of the solution.) These ripples seem to travel faster than the main pulse at this stage and, due to periodicity, wrap around the boundary and superimpose themselves on the rest of the solution. Their amplitude in the beginning is slowly rising with time. Of course, one cannot rule out categorically that the change in amplitude is not because of a long-time linear error growth due to the numerical integration. It is worth noting, though, that when the computations are repeated with different discretization parameters, using splines of different degrees in space and other types of temporal discretizations (some of which are of dissipative type), there the same profile at the same value of t and level of cleaning was obtained exactly. However, as we are not solving the nonlinear system of the fully discrete scheme exactly, but are using instead Newton’s method and solving the associated linear systems iteratively, some slow error growth is expected in long time computations (see, e.g. [12]). Observe, however, that, as time advances, the maximum amplitude of the ripples tends to stabilize. So does the amplitude of the main pulse as well. Therefore, one could ask whether this procedure will eventually yield a main pulse and ripples of constant amplitude travelling at the same speed, i.e. a travelling wave of the GSW type. It is difficult to check numerically a ‘pointwise’ travelling-wave property for profiles like those of figure 6, given the difficulty in measuring precisely the speed and the amplitude of the main pulse and of the ripples.

In the next section, the generation of ripples is further studied in other examples, posed in larger spatial intervals with ripples of larger size, in which the decay of the main pulse (in L^∞ and also in L^2) is clearly observed.

4. Radiation of ripples

In this section, the outcome of some numerical experiments is presented; they focus on the initial stages of the generation of ripples when a solitary-wave-like pulse evolves according to the system (1.1) or (1.2). Although we still integrate the periodic initial-value problem, larger spatial intervals are taken to simulate more accurately the Cauchy problem evolution of the ripples and the main pulse over a longer temporal interval.

As a preliminary note of interest, consider the change in variables $x \rightarrow y = x - c_s t$, where $c_s > 1$ denotes the speed with which a main, solitary-wave-like pulse of the system (1.1) or (1.2) travels to the right. Then small-amplitude solutions evolve in a frame travelling with this main pulse according to the linearization of (1.1) or (1.2), i.e. according to the constant coefficient system

$$\begin{aligned}(\partial_t - c_s \partial_y)\eta + \partial_y \left(1 + \frac{1}{6} \partial_{yy}\right)u &= 0, \\(\partial_t - c_s \partial_y)u + \partial_y \left(1 + \frac{1}{6} \partial_{yy}\right)\eta &= 0.\end{aligned}$$

Combining the above equations, it is observed that η and u satisfy the equation

$$(\partial_t - c_s \partial_y)^2 \eta - \left(\partial_y \left(1 + \frac{1}{6} \partial_{yy}\right)\right)^2 \eta = 0,$$

which has solutions of the form $\eta(y, t) = e^{i(\kappa y - \omega_{\pm}(\kappa)t)}$, $\kappa \in \mathbb{R}$, that satisfy the dispersion relation

$$\omega_{\pm}(\kappa) = -c_s \kappa \pm \kappa \left(1 - \frac{1}{6} \kappa^2\right).$$

Thus, the phase speed $v_{\pm} = \omega_{\pm}/\kappa$ is given by

$$v_{\pm}(\kappa) = -c_s \pm \left(1 - \frac{1}{6} \kappa^2\right).$$

Observe that for large enough wavenumbers $\kappa > \sqrt{6(c_s + 1)}$, there is a solution component of the form $e^{i(\kappa y - \omega_{-}(\kappa)t)}$ which is leading the solitary pulse (i.e. its phase speed v_{-} is positive in this coordinate system). This is an indication that we may expect the existence of outward-propagating ripples in front of the main pulse. (For smaller κ , v_{-} becomes negative; this is an indication of the existence of a dispersive tail trailing the main pulse). It is worth noting that for large κ the group velocity of the oscillations is given in this frame of reference by

$$\frac{d}{d\kappa} \omega_{-}(\kappa) = -c_s - 1 + \frac{1}{2} \kappa^2.$$

Thus, it exceeds the phase speed $v_{-}(\kappa)$ by $\frac{1}{3} \kappa^2$. (This can be observed in the evolution depicted in figures 6(a) and (b), where a phase speed of 1.11 (in the original x, t frame of reference) corresponding to $\kappa = 3.55$ gives a group velocity of 5.31, which would place the front of the ripples at $t = 40$ at about $x = 126$, in approximate agreement with what is observed in figure 6(b).)

To study the onset of the ripples, the integration was carried out on the much larger spatial interval $[-750, 750]$. The symmetric KdV–KdV system (1.2) was integrated on this interval using the evolution code with cubic splines and $h = 0.1, k = 0.02$. (We obtained qualitatively similar results for the usual KdV–KdV system (1.1). However, as the emerging ripples for the latter system are of smaller amplitude, the radiation phenomena are easier to describe in the context of the symmetric system.) The initial conditions η_0 and u_0 were chosen as in [1, 8] to provide approximately unidirectional profiles. (This enables one to dispense with much cutting and cleaning. In addition, we observed that such one-way initial profiles produce larger size ripples during their evolution, with consequent measurement advantages.) The particular initial data taken were

$$\eta_0(x) = \phi(x), \quad tqsu_0(x) = \phi(x) + \frac{1}{4} \phi^2(x), \tag{4.1}$$

where $\phi(x) = A \operatorname{sech}^2\left(\frac{\sqrt{3}A}{2}x\right)$ is a solitary-wave solution of the KdV equation $u_t + u_x + \frac{3}{2}uu_x + \frac{1}{6}u_{xxx} = 0$. When $A = 0.6$, the η -component of the numerical solution is shown for $t = 0(100)500$ in the sequence of plots in figure 9.

The computation is of very good quality. The invariants

$$\int_{-750}^{750} \eta \, dx = 1.788\,854\,382\,00, \quad \int_{-750}^{750} u \, dx = 1.967\,739\,820\,19,$$

$$\int_{-750}^{750} (u^2 + \eta^2) \, dx = 1.613\,853\,313\,31$$

maintain the 11 digits shown up to $t = 500$. The waveform that emerges indeed moves mainly to the right, shedding a tiny dispersive tail that trails the main pulse. It consists of two parts travelling in both directions reflecting the fact that the system models two-way propagation. Ripples of large size, of maximum amplitude a equal to about 0.03, appear at the front of the

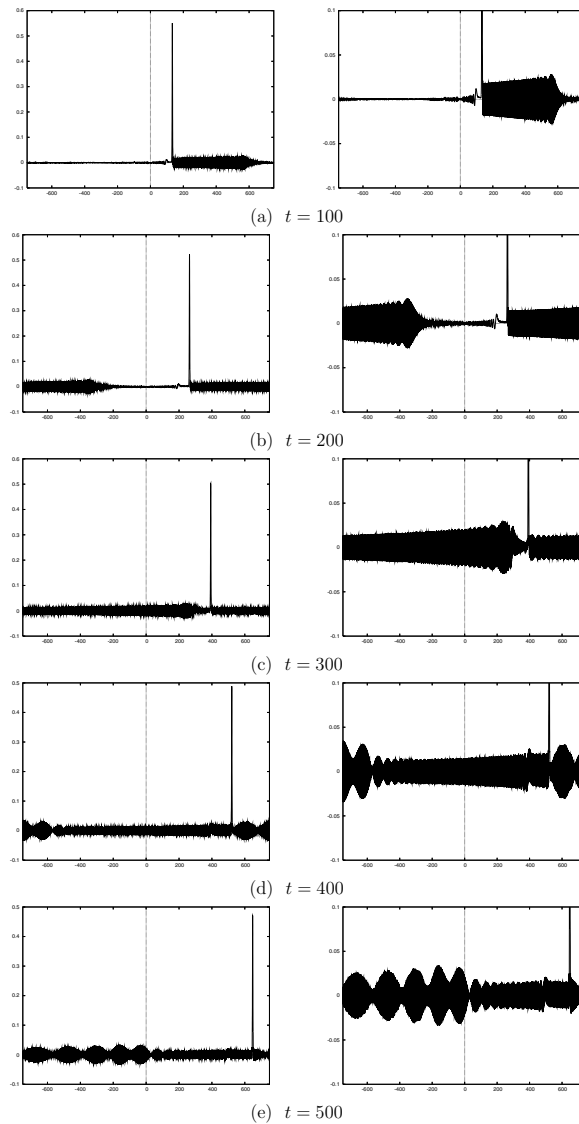


Figure 9. Evolution of the η -component of the solution, symmetric KdV–KdV system, initial data (4.1), $A = 0.6$. The plots on the right are magnifications of those on the left. (a) $t = 100$, (b) $t = 200$, (c) $t = 300$, (d) $t = 400$ and (e) $t = 500$.

main pulse and are radiated to the right. (They qualitatively resemble the ripples shown in the figures of [6] and [4], where the unidirectional fifth-order KdV equation was integrated numerically). By $t = 300$, the ripples have propagated through the boundary and are starting to interact with the dispersive tail and the main pulse. (It is interesting to note that very small ripples apparently emanate from the dispersive tail as well.)

As a result of the formation of large ripples, the amplitude of the main pulse clearly decays, as in figure 10. The oscillations after about $t = 300$ are due to the interactions of the ripples with the rest of the solution. Figure 11 shows a similar type of temporal decay for the quantity $E_\eta(t) := \int_{\{x: \eta(x,t) > 0.02\}} \eta^2(x,t) dx$, which approximates the ‘energy’, i.e. the

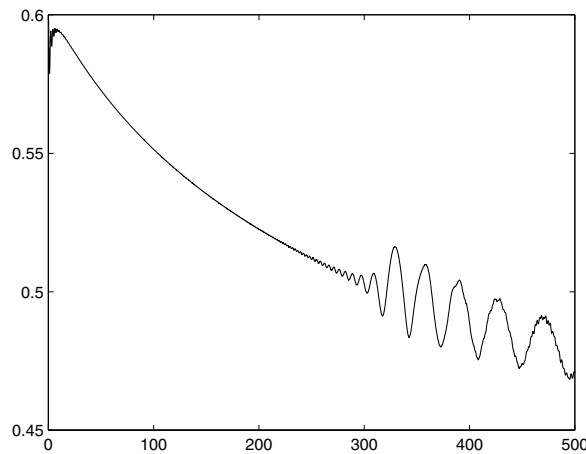


Figure 10. Amplitude of the η -component of the solution as a function of t ; evolution of figure 9.

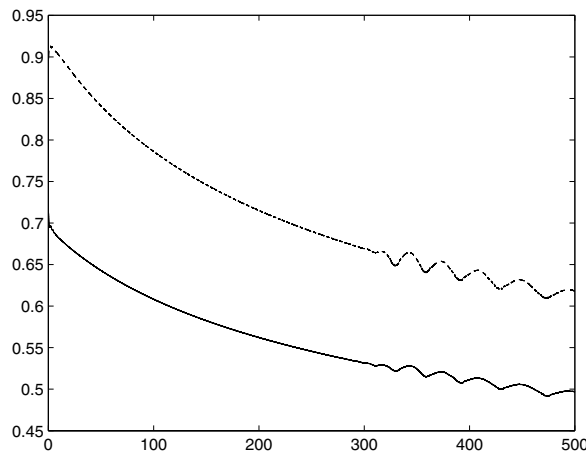


Figure 11. ‘Energy’ E_η (—) and E_u (- - -) of η and u of the main pulse as a function of t ; evolution of figure 9.

square of the L^2 -norm of the elevation of the main pulse, as well as the decay of the analogous ‘energy’ functional $E_u(t) = \int_{\{x: \eta(x,t) > 0.02\}} u^2(x, t) dx$ of the u -component of the main pulse. The analogous ‘energy’ of the ripples, defined as $E_{\text{rip}}(t) = \int_{\{x: \eta(x,t) \leq 0.02\}} (u^2 + \eta^2) dx$, is of course increasing; its graph is shown as a function of t in figure 12.

As already mentioned, the KdV–KdV system (1.1) gives qualitatively similar results. (Note that the correct one-way initial data for (1.1) are $\eta_0(x) = \phi(x)$, $u_0(x) = \phi - \frac{1}{4}\phi^2$.)

Table 1 shows, in the cases of a few experiments that were run for both systems, the values of the amplitude A , the maximum value of the KdV solitary wave that we took as η_0 and the resulting observed approximate maximum amplitude a of the η -component of the ripples after they have been fully established and before they have interacted with the rest of the solution due to periodicity. Observe that for small initial amplitude A , the size of the emerging ripples is extremely small, while the size of the ripples increases rapidly with A . (In the case of the fifth-order KdV equation, asymptotic computations in [6] and [4], and also in [29], show

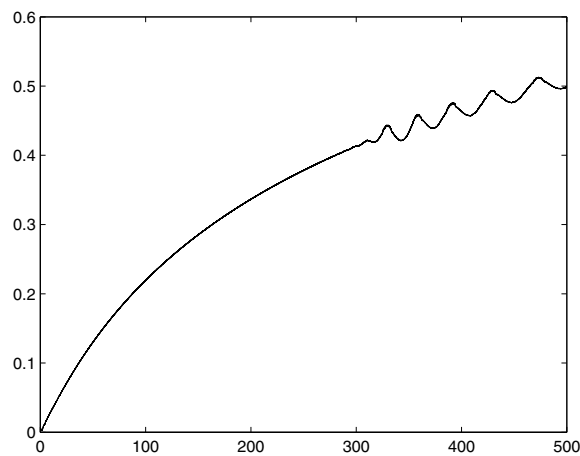


Figure 12. ‘Energy’ of the ripples E_{rip} as a function of t ; evolution of figure 9.

Table 1. Amplitude A of η_0 and resulting maximum amplitude a of ripples; KdV–KdV system (1.1) and symmetric KdV–KdV system (1.2).

A	a (1.1)	a (1.2)
0.2	2×10^{-5}	6×10^{-5}
0.3	0.0004	0.0009
0.4	0.0016	0.004
0.6	0.0086	0.027
0.8	0.022	0.08
1.0	0.042	0.14
1.2	Blow-up	0.2

that a decreases exponentially as A decreases.) For $A \geq 1.2$ the numerical solution of (1.1) appeared to form a single-point blow-up singularity in finite time caused by the growth of the negative excursion of the ripples which at some point becomes less than -1 , drying the channel locally and rendering the KdV–KdV models completely invalid. We cannot be certain, using a uniform mesh evolution code, whether this is a numerical artefact or a property of the solution of the problem. However, when the computations were repeated with smaller h and k and quintic splines, blow-up occurred at about the same value of t . No blow-up was observed in the case of the symmetric system (1.2) for the same ranges of A and temporal intervals of integration, however.

In conclusion, on the basis of our numerical experiments, it is reasonable to conjecture that in the case of the pure initial-value problem for the KdV–KdV systems, localized initial conditions of finite L^2 -norm will resolve themselves, as time grows, into a principal structure consisting of solitary-wave-like pulses and dispersive tails and another part consisting of radiated, outgoing wavetrains of ripples. The main part of the solution will decay in amplitude and eventually (although we did not reach that stage in our computations) all its energy will be transferred to the ripples that will probably disperse as $t \rightarrow \infty$.

5. Interactions and ‘stability’ of solitary-wave-like solutions of the KdV–KdV systems

Reported in this section are computational experiments performed to shed light on interaction and ‘stability’ of solitary-wave-like solutions (radiating solitary waves and GSWs) of the

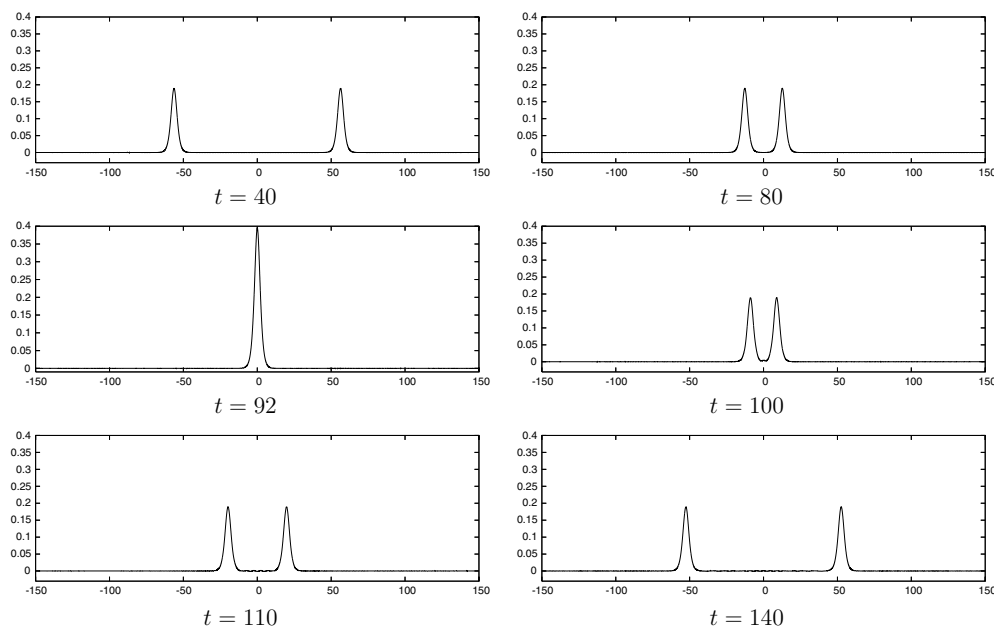


Figure 13. Collision of ‘cleaned’ pulses of system (1.1); the η -profiles.

KdV–KdV systems (1.1) and (1.2). Such phenomena have been extensively studied for classical solitary waves, by numerical and analytic techniques in the case of one-way models such as the KdV or the BBM equation and their generalized analogs and by numerical means in the case of other Boussinesq systems (cf, e.g. [2, 8, 12, 14, 20, 21, 28]). The aim is to describe what happens in some analogous situations in the case of the KdV–KdV systems. For both systems the results were qualitatively similar, so the outcome is reported for only one case.

5.1. Head-on collisions

The first configuration considered is *interaction during a head-on collision* of two radiating solitary waves. We report two numerical experiments. Consider the system (1.1) with initial values of the form $\eta(x + 100) + \eta(x - 100)$ and $u(x + 100) - u(x - 100)$, where η and u are ‘cleaned’ pulses obtained from a Gaussian as described in section 3. The evolution derived from this starting point is shown in figure 13. Figure 14 shows a magnification of two profiles of figure 13 that enable one to see some details of the interaction. As t grows, but still prior to the interaction, tiny ripples appear in front and behind (due to periodicity) the main pulses, as expected from the experiments of section 3. After the main pulses collide at about $t = 92$ and pass through each other, there is an interaction of the dispersive tails following the two main pulses as they separate and an enlargement of the ripples in front of them (figure 14, right).

Figure 15(a) shows the (total) amplitude of the solution as a function of t for this experiment. During the interaction the amplitude rises to about 0.398 33, which is approximately 5.21% above the sum of the amplitudes of the two initial pulses, and returns to its previous value modulo small oscillations due to ripples. Figure 15(b) is a phase shift diagram showing the paths in the x – t plane of the two main pulses. As in the case of collisions of classical solitary waves, the main pulses are slightly delayed by the interaction.

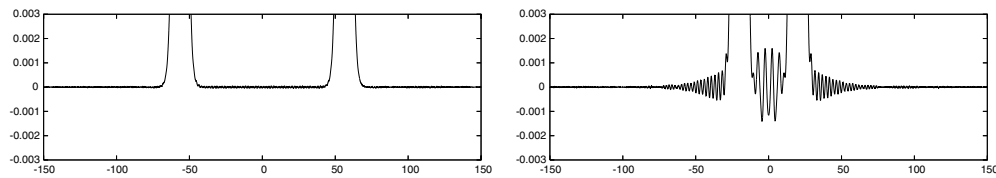


Figure 14. Magnification of profiles in figure 13 at $t = 40$ and $t = 110$.

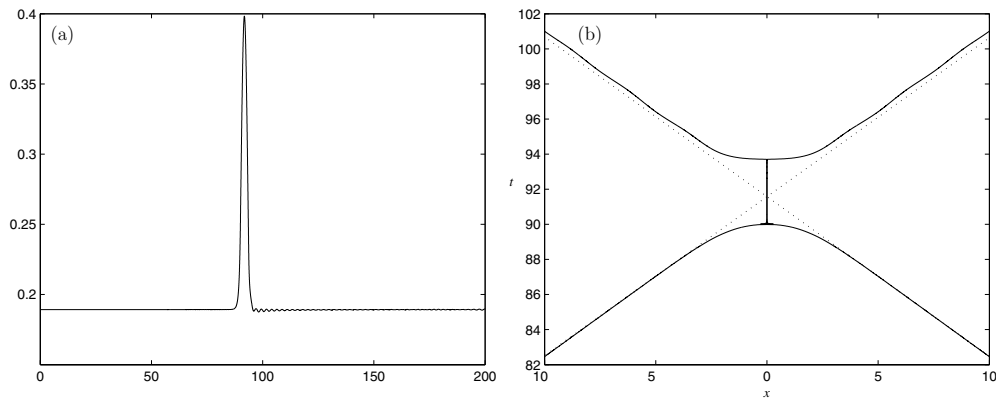


Figure 15. Total amplitude and phase shift diagram for the head-on collision of figure 13.

In another numerical experiment, we took as initial values for the system (1.1) the *exact* GSWs of the KdV–KdV system obtained as solutions of the periodic two-point boundary-value problem for the appropriate system of nonlinear ordinary differential equations that arise from the KdV–KdV system upon making a travelling-wave assumption and which were analysed in section 4 of [13]. As was pointed out in [13], the evolution code perfectly preserves the GSWs as travelling-wave solutions. Figure 16 shows what happens when two such GSWs collide. The spatial interval was taken to be $[-50, 50]$ and the initial η profiles were centred at $x = \pm 20$ and given opposite velocities. (The GSWs have speed 1.2, i.e. $c = 0.2$ in the notation of section 4 of [13], and were constructed with half-period $L = 50$.) The simulation of their temporal evolution was accomplished with cubic splines and $h = 0.05$, $k = 0.01$. The features of the collision are basically the same as those shown in figure 13, but the oscillations produced after the interactions are larger. Figure 17 shows the evolution of the total amplitude of the solution and the phase shift diagram near the collision point. For this experiment, the GSWs cease to be GSWs after the interaction and they apparently become radiating solitary waves. Thus, they do not seem to be stable as GSWs under this interaction, in contrast to what happens to classical solitary-wave solutions of one-way model equations or of other Boussinesq systems.

5.2. Perturbations of initial GSWs

We pursue further the issue of ‘instability’ of GSWs for the KdV–KdV systems raised by the previous experiment by studying computationally the evolution of slightly perturbed GSWs of (1.1). It was seen, for example, in [20] that classical solitary waves of other Boussinesq systems appear, in similar computational experiments, to be asymptotically stable. However, it seems that GSWs become radiating solitary waves when subjected to small perturbations.

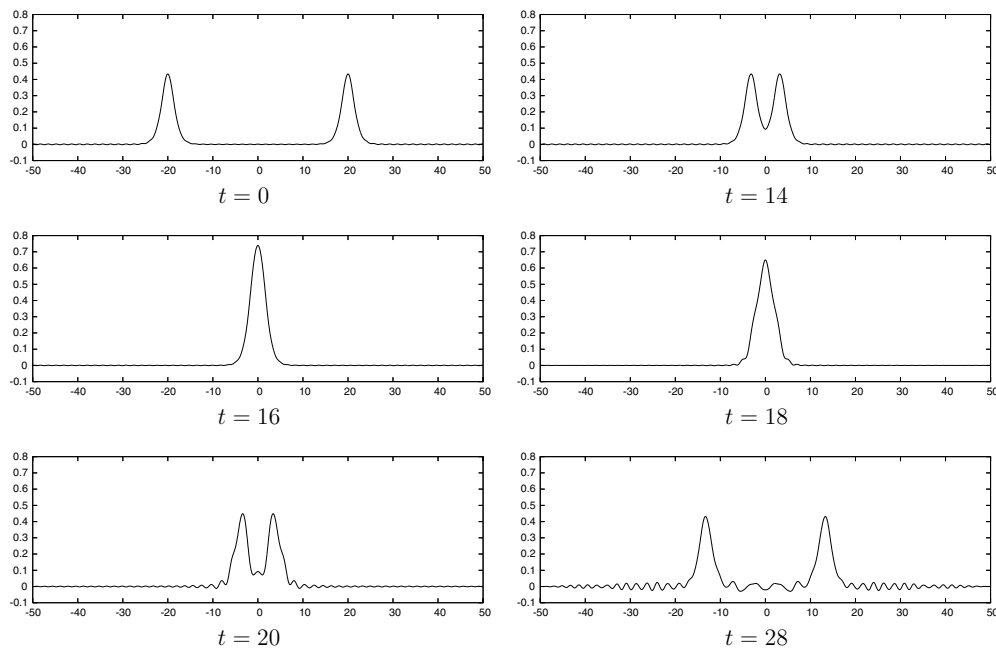


Figure 16. Collision of two initially exact GSWs for system (1.1); η components.

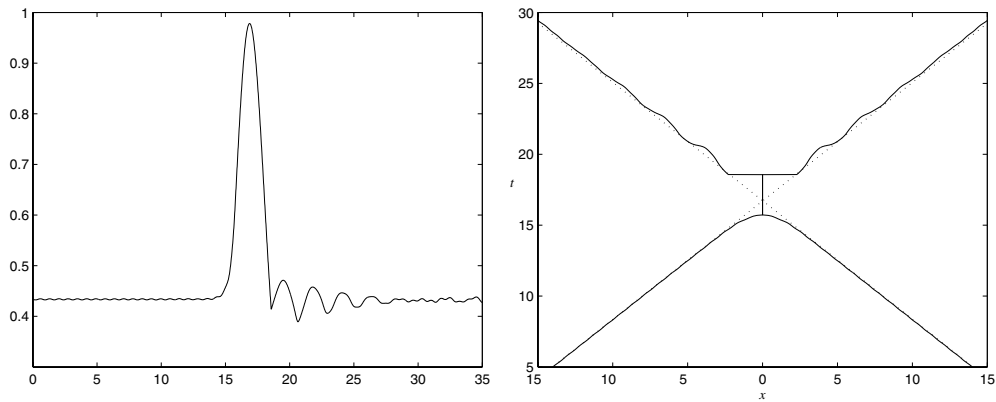


Figure 17. Total η amplitude versus time and phase shift diagram for the collision of the GSWs in figure 16.

This is illustrated in numerical experiments in which we took as η_0 and u_0 a GSW pair for the system (1.1) generated by solving the periodic two-point boundary-value problem for the ordinary differential equations that result from the travelling-wave hypothesis. (These were GSWs with speed $c_s = 1.2$ ($c = 0.2$), constructed with $L = 150$.) The perturbed initial data $(\tilde{\eta}_0, \tilde{u}_0)$ were taken to be $\tilde{\eta}_0(x) = r\eta_0(x)$ and $\tilde{u}_0(x) = u_0(x)$, where r is a perturbation parameter. Figure 18 shows the evolution in the case $r = 1.05$. The main pulse travels to the right. As a result of the small perturbation, dispersive tails appear travelling to the left and right, as expected from similar experiments in the case of classical solitary waves in [20]. In addition, new ripples of larger amplitude emerge mainly in front of the main pulse. They

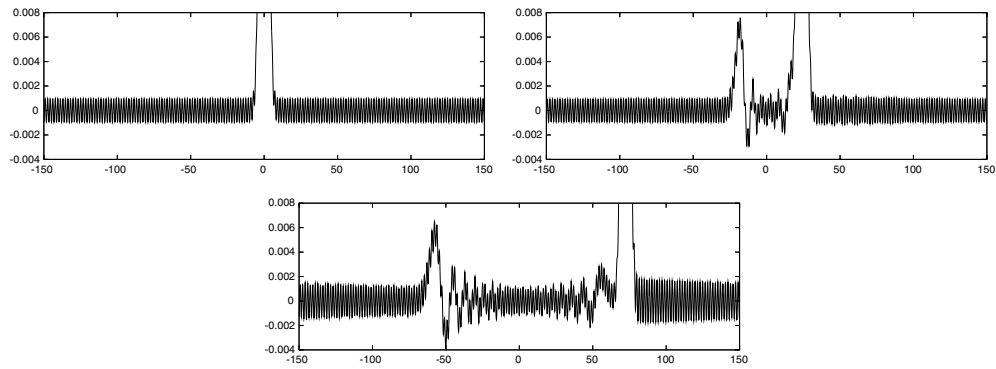


Figure 18. Evolution of a perturbed GSW for (1.1). Perturbation of $\eta_0(x)$, $r = 1.05$, $t = 0, 20, 60$.

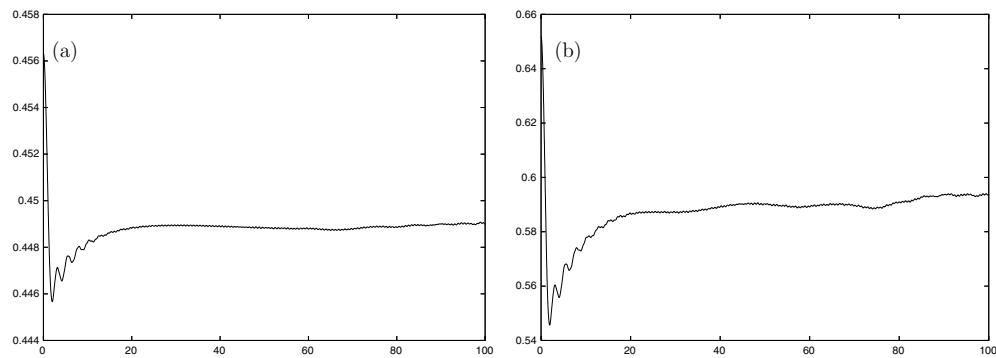


Figure 19. Evolution of the amplitude of the main pulse, figures 18 and 20. (a) $r = 1.05$, (b) $r = 1.5$.

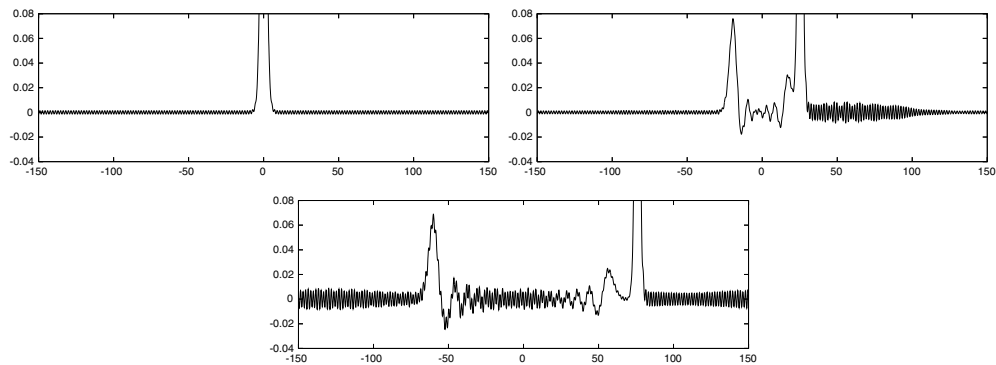


Figure 20. Evolution of a perturbed GSW for (1.1); $\tilde{\eta}_0(x) = r\eta_0(x)$ with, $r = 1.5$, $t = 0, 20, 60$.

superimpose themselves on the dispersive tail as well. Figure 19(a) shows the evolution of the amplitude of the main pulse. When the perturbation factor r grows to 1.5 (figures 20 and 21) the emerging ripples in front of the main pulse become larger in amplitude. Figure 19(b) shows the associated evolution of the amplitude of the larger main pulse as a function of time.

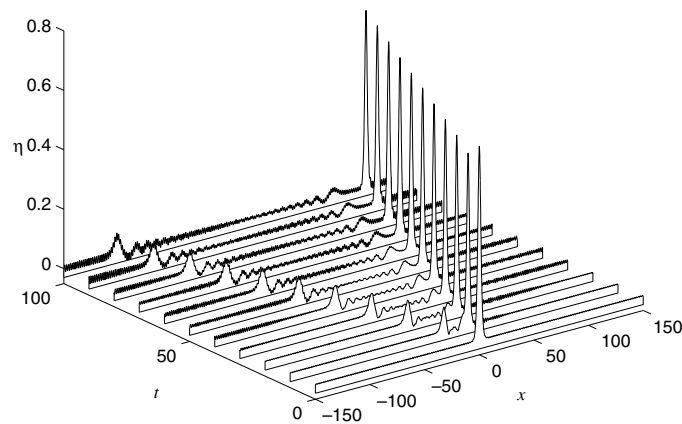


Figure 21. Perspective view of the evolution of the perturbed GSW of (1.1) with $r = 1.5$.

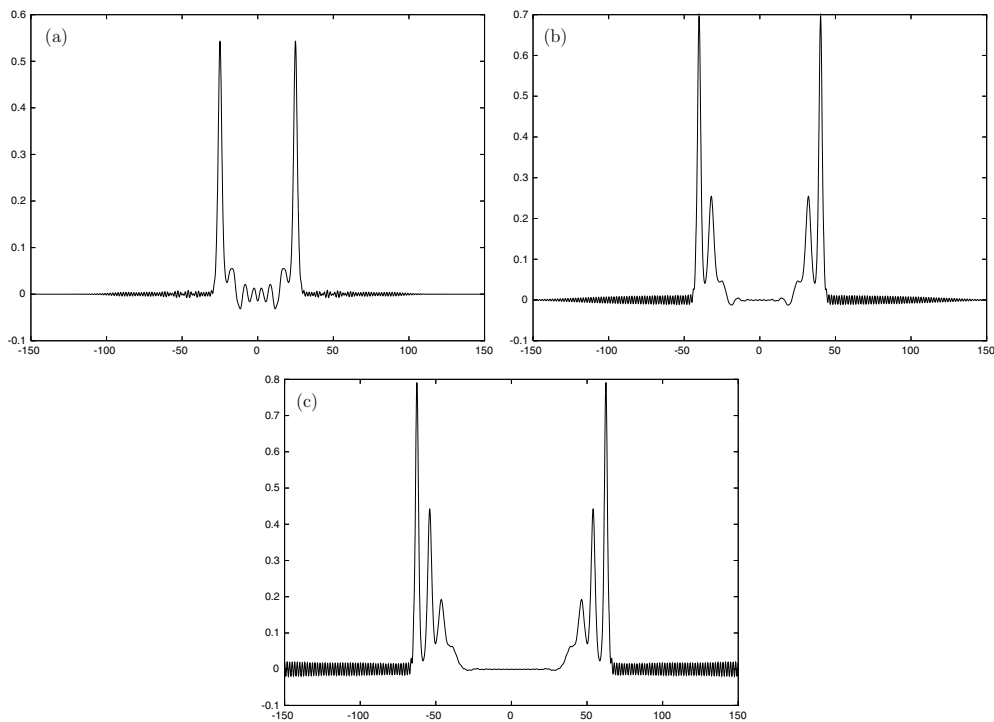


Figure 22. Resolution of a Gaussian; system (1.1), $a_0 = 1$, (a) $\lambda = 1/5$ ($t = 20$), (b) $\lambda = 1/15$ ($t = 30$), (c) $\lambda = 1/35$ ($t = 45$).

5.3. Sequences of radiating solitary waves produced from general initial profiles

Another manifestation of the stability of classical solitary waves is the *resolution property* of arbitrary, suitably decaying initial profiles into sequences of solitary waves plus dispersive tails. This property has also been studied in detail by inverse scattering techniques in the case of the KdV equation and by means of numerical experiments in a variety of non-integrable, unidirectional equations and in Boussinesq systems, see, e.g. [12, 20, 28]. In the case of the

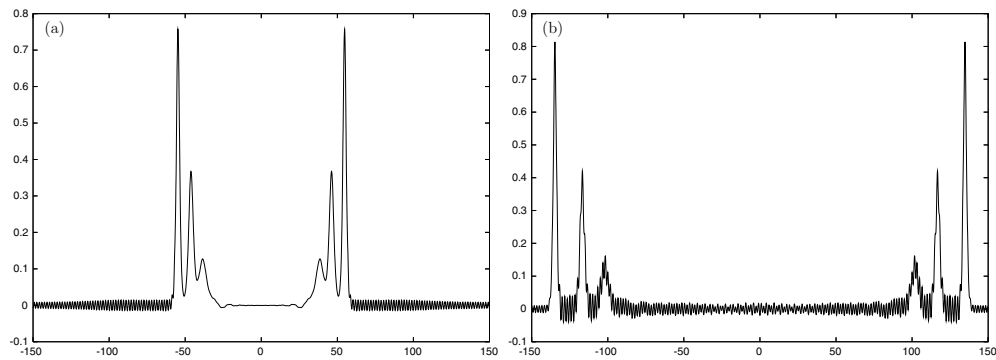


Figure 23. Resolution of a Gaussian; system (1.1), $a_0 = 1$, $\lambda = 1/25$ (a) $t = 40$, (b) $t = 100$.

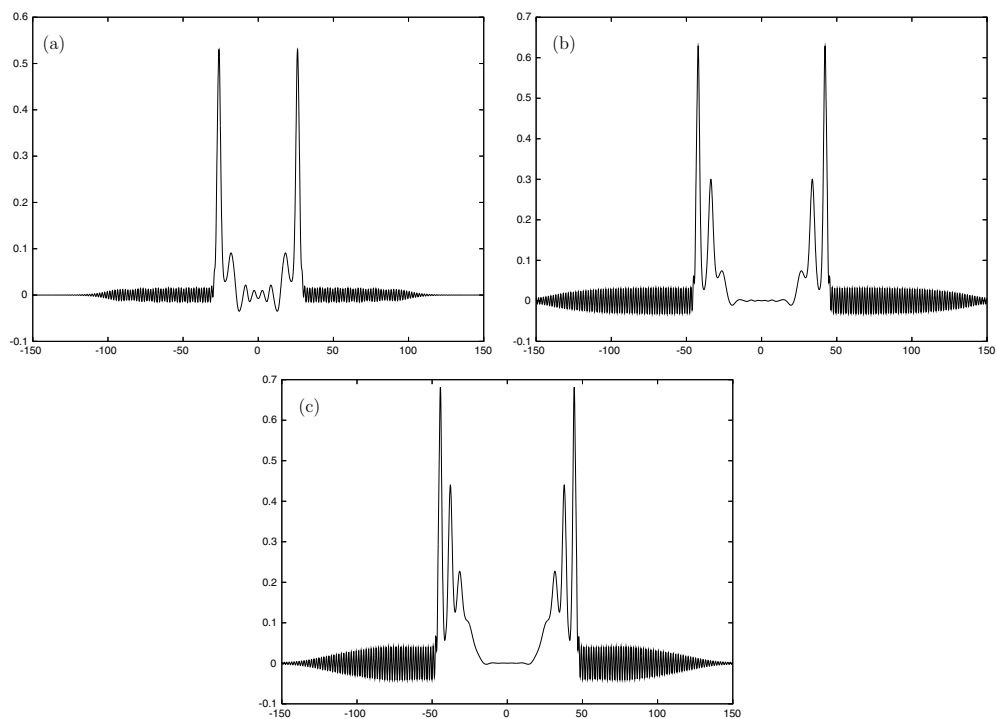


Figure 24. Resolution of a Gaussian; system (1.2), $a_0 = 1$, (a) $\lambda = 1/5$ ($t = 10$), (b) $\lambda = 1/15$ ($t = 15$), (c) $\lambda = 1/35$ ($t = 15$).

KdV–KdV systems, an example of the resolution of a Gaussian initial condition into radiating solitary waves was already observed in section 3. Pursuing this issue further, we considered the system (1.1) and took initial data of the form $\eta_0(x) = a_0 e^{-\lambda x^2}$, $u_0(x) = 0$ in $[-150, 150]$. With such initial conditions, it was observed that the initial profile resolves into leftward- and rightward-travelling sequences of solitary-wave-like pulses whose number depends on the parameters a_0 and λ of the initial Gaussian, together with trailing dispersive tails, see figures 22 and 23. In the beginning, ripples are radiated only in front of the front running main pulses of each wavetrain. Subsequently, the whole profile is polluted by them due to

periodicity, e.g. figure 23(b). A similar picture is obtained for the symmetric system (1.2), albeit with larger ripples, see figure 24. When we took a larger amplitude a_0 in the Gaussian (for example, for $a_0 = 2$) the numerical solution of (1.1) appeared to blow up in finite time. It is uncertain whether this is a numerical or a real phenomenon. However, the experiment was repeated with smaller mesh parameters h and k and blow-up was observed at the same time. It is also relevant that no blow-up was observed for the symmetric KdV–KdV system (1.2) for the same initial disturbances.

Acknowledgments

The work of Dougalis and Mitsotakis was partly supported by a ‘Pythagoras’ grant to the University of Athens, co-funded by the Ministry of National Education, Greece, and the European Social Fund of the E.U. The work of Bona was supported by the National Science Foundation, USA.

References

- [1] Alazman A A, Albert J P, Bona J L, Chen M and Wu J 2006 Comparisons between the BBM equation and a Boussinesq system *Adv. Diff. Eqns* **11** 121–66
- [2] Antonopoulos D C, Dougalis V A and Mitsotakis D E 2008 Numerical solution of Boussinesq systems of the Bona-Smith type (*preprint*) to be submitted
- [3] Amick C J and Toland J F 1992 Solitary waves with surface tension: I. Trajectories homoclinic to periodic orbits in four dimensions *Arch. Ration. Mech. Anal.* **118** 37–69
- [4] Bakholdin I and Il’ichev A 1996 Radiation and modulational instability described by fifth-order Korteweg–de Vries equation *Contemp. Math.* **200** 1–15
- [5] Beale J T 1991 Exact solitary water waves with capillary ripples at infinity *Commun. Pure Appl. Math.* **44** 211–47
- [6] Benilov E S, Grimshaw R and Kuznetsova E P 1993 The generation of radiating waves in a singularly-perturbed Korteweg–de Vries equation *Physica D* **69** 270–8
- [7] Bona J L 1981 Convergence of periodic wavetrains in the limit of large wavelength *Appl. Sci. Res.* **37** 21–30
- [8] Bona J L and Chen M 1998 A Boussinesq system for two-way propagation of nonlinear dispersive waves *Physica D* **116** 191–224
- [9] Bona J L, Chen M and Saut J-C 2002 Boussinesq equations and other systems for small-amplitude long waves in nonlinear dispersive media: I. Derivation and linear theory *J. Nonlinear Sci.* **12** 283–318
- [10] Bona J L, Chen M and Saut J-C 2004 Boussinesq equations and other systems for small-amplitude long waves in nonlinear dispersive media: II. The nonlinear theory *Nonlinearity* **17** 925–52
- [11] Bona J L, Colin T and Lannes D 2005 Long wave approximations for water waves *Arch. Ration. Mech. Anal.* **178** 373–410
- [12] Bona J L, Dougalis V A, Karakashian O A and McKinney W R 1995 Conservative, high-order numerical schemes for the generalized Korteweg–de Vries equation *Phil. Trans. R. Soc. Lond. A* **351** 107–64
- [13] Bona J L, Dougalis V A and Mitsotakis D E 2007 Numerical solution of KdV–KdV systems of Boussinesq equations: I. The numerical scheme and existence of generalized solitary waves *Math. Comput. Simulation* **74** 214–28
- [14] Bona J L, McKinney W R and Restrepo J M 2000 Stable and unstable solitary-wave solutions of the generalized regularized long-wave equation *J. Nonlinear Sci.* **10** 603–38
- [15] Boyd J P 1991 Weakly non-local solitons for capillary-gravity waves: fifth-degree Korteweg–de Vries equation *Physica D* **48** 129–46
- [16] Champneys A R and Lord G J 1997 Computation of homoclinic solutions to periodic orbits in a reduced water-wave problem *Physica D* **102** 101–24
- [17] Champneys A R, Vanden-Broeck J-M and Lord G J 2002 Do true elevation gravity-capillary solitary waves exist? A numerical investigation *J. Fluid. Mech.* **454** 403–17
- [18] Chen H 2006 Long-period limit of nonlinear dispersive waves: the BBM-equation *Diff. Integr. Eqns* **19** 463–80
- [19] Dias F and Iooss G 2003 Water-waves as a spatial dynamical system *Handbook for Mathematical Fluid Dynamics* ed S Friedlander and D Serre (Amsterdam: Elsevier) pp 443–99
- [20] Dougalis V A, Duran A, Lopez-Marcos M A and Mitsotakis D E 2007 A numerical study of the stability of solitary waves of the Bona-Smith system *J. Nonlinear. Sci.* **17** 569–607

- [21] Mitsotakis D E 2007 Theory and numerical analysis of nonlinear dispersive wave equations: Boussinesq systems in one and two dimensions *PhD Thesis* University of Athens (in Greek)
- [22] Grimshaw R and Iooss G 2003 Solitary waves of a coupled Korteweg–de Vries system *Math. Comput. Simulation* **62** 31–40
- [23] Grimshaw R and Joshi N 1995 Weakly nonlocal solitary waves in a singularly perturbed Korteweg–de Vries equation *SIAM J. Appl. Math.* **55** 124–35
- [24] Hunter J K and Scheurle J 1988 Existence of perturbed solitary wave solutions to a model equation for water waves *Physica D* **32** 253–68
- [25] Hunter J K and Vanden-Broeck J-M 1983 Solitary and periodic gravity-capillary waves of finite amplitude *J. Fluid Mech.* **134** 253–68
- [26] Lombardi E 2000 Oscillatory integrals and phenomena beyond all algebraic orders, with applications to homoclinic orbits in reversible systems *Lecture Notes in Mathematics* vol 1741 (Berlin: Springer)
- [27] Michallet H and Dias F 1999 Numerical study of generalized interfacial waves *Phys. Fluids* **11** 1502–11
- [28] Pelloni B and Dougalis V A 2001 Numerical modelling of two-way propagation of non-linear dispersive waves *Math. Comput. Simulation* **55** 595–606
- [29] Pomeau Y, Ramani A and Grammaticos B 1988 Structural stability of the Korteweg–de Vries solitons under a singular perturbation *Physica D* **31** 127–34
- [30] Sun S M 1991 Existence of a generalized solitary wave with positive Bond number smaller than $\frac{1}{3}$ *J. Math. Anal. Appl.* **156** 471–504
- [31] Vanden-Broeck J-M 1991 Elevation solitary waves with surface tension *Phys. Fluids A* **11** 2659–63
- [32] Yang T-S and Akylas T R 1996 Weakly nonlocal gravity-capillary solitary waves *Phys. Fluids* **8** 1506–14